Elliptical modulation and temporal decays of near-inertial surface currents under submesoscale horizontal shear and strain components in a coastal region

Sung Yong Kim[1,†]

[1]Department of Mechanical Engineering, Korea Advanced Institute of Science and Technology, syongkim@kaist.ac.kr[†]

Abstract

We investigate elliptical modulations and modified temporal decays of near-inertial coastal surface currents in the observations of coastal-radar-derived submesoscale surface currents and satellite-tracked surface drifters as well as forward realistic coastal circulation simulations off the Oregon coast in terms of the influence of horizontal shear and strain components. The elliptical near-inertial surface currents appear with dominant clockwise and non-negligible counter-clockwise near-inertial variance, and their temporal decays are enhanced in fall and winter compared with those in spring and summer, especially near the coast (25 to 50 km from the coast), with seasonal variability. We formulate a slab layer model to explain the potential contribution of submesoscale horizontal shear and strain components to the near-inertial motions, along with anisotropic constant frictional coefficients under wind-driven coastal dynamics. The horizontal shear components, including the background vorticity associated with submesoscale eddies, contribute to the elliptical near-inertial currents, reduce the regionally dominant polarization, and correct the effective Coriolis frequency up to a half of the local Coriolis frequency compared with that in the modulation of near-inertial currents due to mesoscale geostrophic currents. The horizontal strain components related to submesoscale ageostrophic currents (e.g., vertical currents due to direct wind-driven upwelling and down-welling, indirect wind stress curl-driven Ekman pumping, and frontal-scale vertical circulation) result in modification of the temporal decay time scales of the near-inertial surface currents, which is an uncounted dynamic component under the non-divergent mesoscale geostrophic currents.

Results

Inertial motions are ubiquitously observed in the open ocean and coastal regions as the resonant dynamical responses of fluids under a rotating coordinate system with a Coriolis frequency [$f = 2\sin\theta$ cycles per day (cpd), where θ denotes the latitude in degree ($-90^\circ \le \theta \le 90^\circ$), and $f > 0$ and $f < 0$ correspond to the Northern Hemisphere and Southern Hemisphere, respectively] to broadband wind stress. These inertial motions are described as purely circular motions in the physical domain with clockwise (counter-clockwise) rotation in the Northern (Southern) Hemisphere. These upper ocean inertial motions can be modulated by background vorticity, including low-frequency currents or geostrophic currents, which are called near-inertial motions, and their energy can be propagated into the ocean interior. The near-inertial motions are valid when (1) the ratio of their vertical to horizontal wavelengths is small and (2) the lower bound of the frequency of the propagating near-inertial internal waves is equal to the inertial frequency.

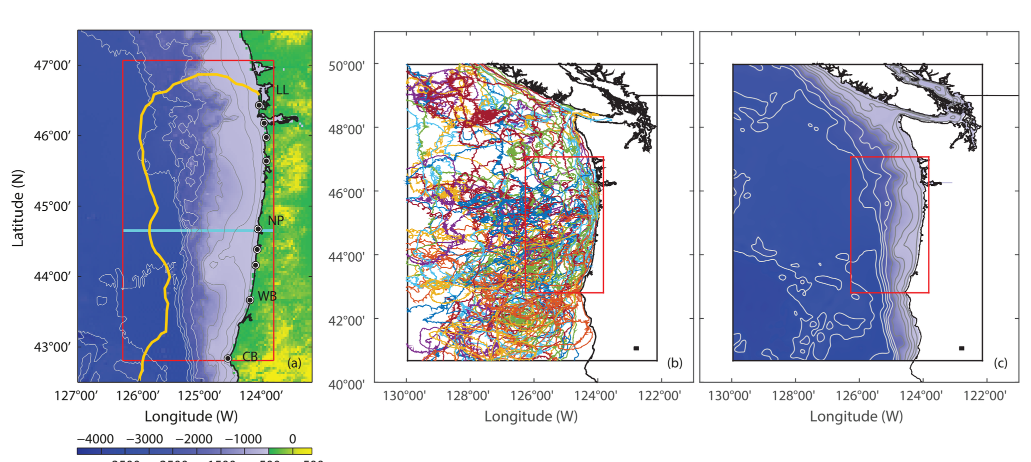

Figure 1: A study domain of elliptical near-inertial surface currents off the coast of Oregon. (a) and (b): Observations of HFR-derived surface currents (11 HFRs as black dots; an effective spatial coverage of HFRs as a yellow contour) and surface drifters (colored individual tracks). The divergence and vorticity at the ocean surface are sampled along a cross-shore line of 44.65°N (cyan; Newport line; NH10) in Fig. 1a to examine their temporal and cross-shore variability. As a reference, major coastal regions are denoted by abbreviated two letter names from south to north. The bottom bathymetry is contoured at 50, 100, 250, 500, 1000, 1500, 2000, 2500, and 3000 m. (c) A domain for the ROMS-simulated surface and subsurface currents and its subset (a red rectangular box).

A slab layer model has been modified to formulate the current responses (u and v) in the upper ocean to wind stress [$\boldsymbol{\tau} = (\tau^x, \tau^y)$] within a mixed layer ($h$):

$$u_t + uu_x + vu_y - fv + r^x u = -\frac{1}{\rho}p_x + \frac{\tau^x}{\rho h}, \tag{1}$$

$$v_t + uv_x + vv_y + fu + r^y v = -\frac{1}{\rho}p_y + \frac{\tau^y}{\rho h}, \tag{2}$$

$$N^2 w = -\frac{1}{\rho}p_{zt}, \tag{3}$$

$$u_x + v_y + w_z = 0, \tag{4}$$

where ρ, r, N and p denote the density of seawater, isotropic frictional coefficient, buoyancy frequency, and pressure, respectively (ρ and $r \in \mathcal{R}$). The subscripts and superscripts indicate the partial derivatives with respect to the given variable (e.g., t, x, y, and z) and the direction in the Cartesian coordinates of the given dynamic variables (e.g., u, v, and τ), respectively. Considering the order of magnitudes in the momentum equations, the pressure gradient terms in Eqs. 1 and 2 depend on the ratio of the vertical scale to squared horizontal scale, which can be ignored if the linear response is dominated by near-inertial motions.

The horizontal momentum equations (Eqs. 1 and 2) are transformed into the frequency domain as follows based on the assumptions and approximations:

$$\left(i\sigma + \frac{R}{b}\right)\hat{u} - \frac{F}{a}\hat{v} = \frac{\hat{\tau}^x}{\rho h}, \tag{5}$$

$$Fa\hat{u} + (i\sigma + Rb)\,\hat{v} = \frac{\hat{\tau}^y}{\rho h}, \tag{6}$$

where $\hat{u}$, $\hat{v}$, $\hat{\tau}^x$, and $\hat{\tau}^y$ denote the Fourier coefficients of u, v, τ^x, and τ^y, respectively.

The extended Coriolis frequency (F), including horizontal shear components (v_x and u_y), as well as the extended frictional coefficient (R), including horizontal strain components (u_x and v_y), and their relevant terms (a and b) are given as,

$$F^2 = (f - u_y)\,(f + v_x)\,, \tag{7}$$

$$R^2 = (r^x + u_x)\,(r^y + v_y)\,, \tag{8}$$

$$a = \sqrt{\frac{f + v_x}{f - u_y}} = \sqrt{\frac{1 + v_x/f}{1 - u_y/f}}, \tag{9}$$

$$b = \sqrt{\frac{r^y + v_y}{r^x + u_x}} = \sqrt{\frac{r^y/f + v_y/f}{r^x/f + u_x/f}}. \tag{10}$$

The polarization (κ) is defined as the ratio of the difference between the near-inertial amplitudes in both rotations to their sum, which allows us (1) to examine the spatial distribution of non-negligible counter-clockwise near-inertial variance and (2) to describe the degrees of circular and elliptical motions of the near-inertial currents,

$$\kappa = \frac{-A^{\mathrm{cw}} + A^{\mathrm{ccw}}}{A^{\mathrm{cw}} + A^{\mathrm{ccw}}}, \tag{11}$$

where A^{cw} and A^{ccw} denote the square roots of the variance of currents in the near-inertial clockwise and counter-clockwise frequency bands, respectively. Zero polarization indicates an equal amount of clockwise and counter-clockwise near-inertial variance and rectilinear motions. Positive and negative polarizations imply the counter-clockwise and clockwise dominance, respectively, and elliptical near-inertial motions.

The polarization of the near-inertial currents is presented in maps (Figs. 2a to 2c) and as a function of the cross-shore distance (Figs. 2d to 2f). The polarization maps of the Eulerian data (e.g., HFR and ROMS) are directly estimated from the rotary kinetic energy spectra of the vector currents at individual grid points (Figs. 2a and 2b).

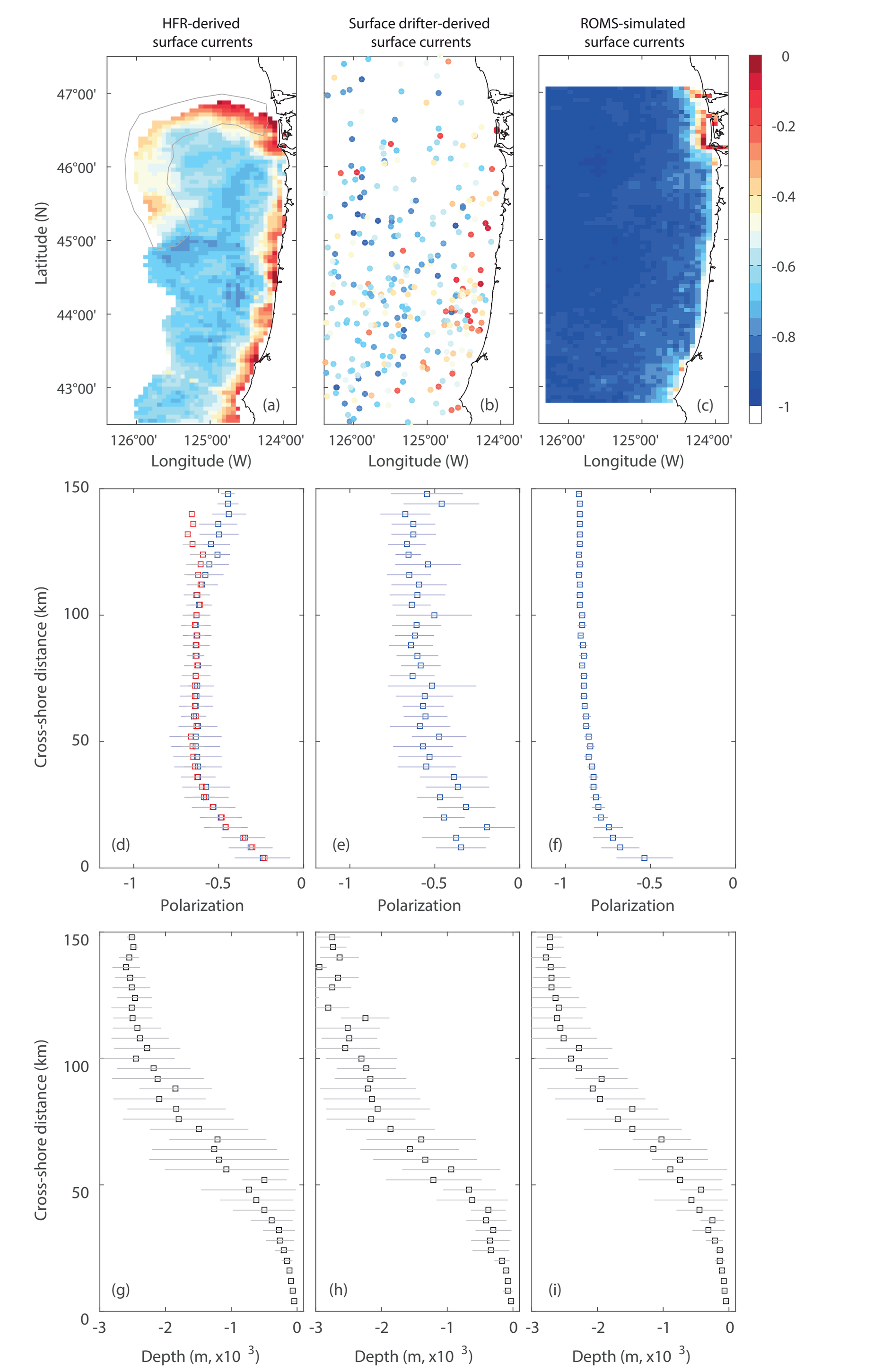

Figure 2: Polarization (κ) of the near-inertial surface currents, obtained from HFRs, surface drifters, and ROMS simulations, and their sampling depths are presented as a map [(a) to (c)] and as a function of cross-shore distance [(d) to (f)]. (g) to (i): Sampling depths (m). (a), (d), and (g): HFRs. (b), (e), and (h): Surface drifters. (c), (f), and (i): ROMS simulations. Figs. 2d to 2i are presented as the means and standard deviations within an equally spaced bin of 4 km in the cross-shore direction. The cross-shore presentation of the polarization is marked with red squares in Fig. 2d when the polarization estimates within a gray contour in Fig. 2a are excluded.

Conversely, the tracks of the Lagrangian drifters are divided into a non-overlapped minimum time series to resolve local near-inertial motions (e.g., 5 days in the study domain), and their rotary kinetic energy spectra are used to compute the polarization of the Lagrangian data (Fig. 2c). The polarization at the coast is close to 0 or -0.5 (Figs. 2a to 2c), which indicates the non-negligible counter-clockwise near-inertial variance, and its cross-shore variations range from nearly -0.2 (HFRs and surface drifters) or -0.5 (ROMS simulations) to -0.8 in the region 50 km from the coast (Figs. 2d to 2f).

The elliptical modulations of near-inertial surface currents can be (1) presented with the amount of frequency shift of the near-inertial peak and (2) quantified with the ratios (α and β in Eqs. 12 and 13) of variance in the subinertial ($f - \delta f/2 \le \sigma \le f$) and super-inertial ($f < \sigma \le f + \delta f/2$) frequency bands to the variance in the near-inertial bandwidth (δf):

$$\alpha(l) = \frac{\sum_{f-\delta f/2 \le \sigma \le f} S(l,\sigma)\Delta\sigma}{\sum_{|\sigma - f| \le \delta f/2} S(l,\sigma)\Delta\sigma}, \tag{12}$$

$$\beta(l) = \frac{\sum_{f < \sigma \le f + \delta f/2} S(l,\sigma)\Delta\sigma}{\sum_{|\sigma - f| \le \delta f/2} S(l,\sigma)\Delta\sigma}. \tag{13}$$

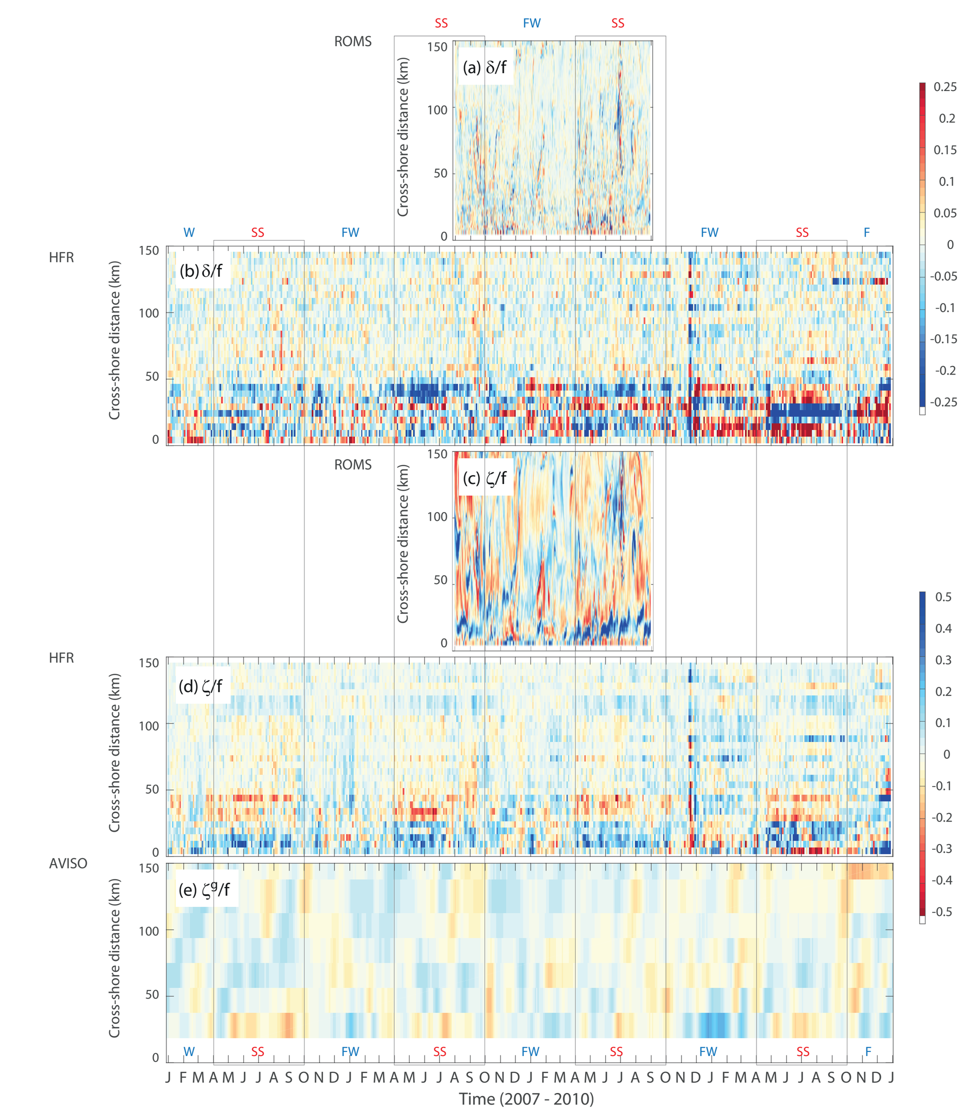

Figure 3: Cross-shore time series of normalized divergence (δ/f) and normalized vorticity (ζ/f) estimated from the [(a) to (d)] submesoscale HFR-derived and ROMS-simulated surface currents and (e) mesoscale geostrophic currents, sampled along the NH10. The time series are generated with a moving average using one day time window and one day increment. (a) and (c): ROMS-simulated surface currents (2 km resolution). (b) and (d): HFR-derived surface currents (6 km resolution). (a) and (b): Normalized divergence (δ/f). (c) to (e): Normalized vorticity (ζ/f and ζ^g/f).

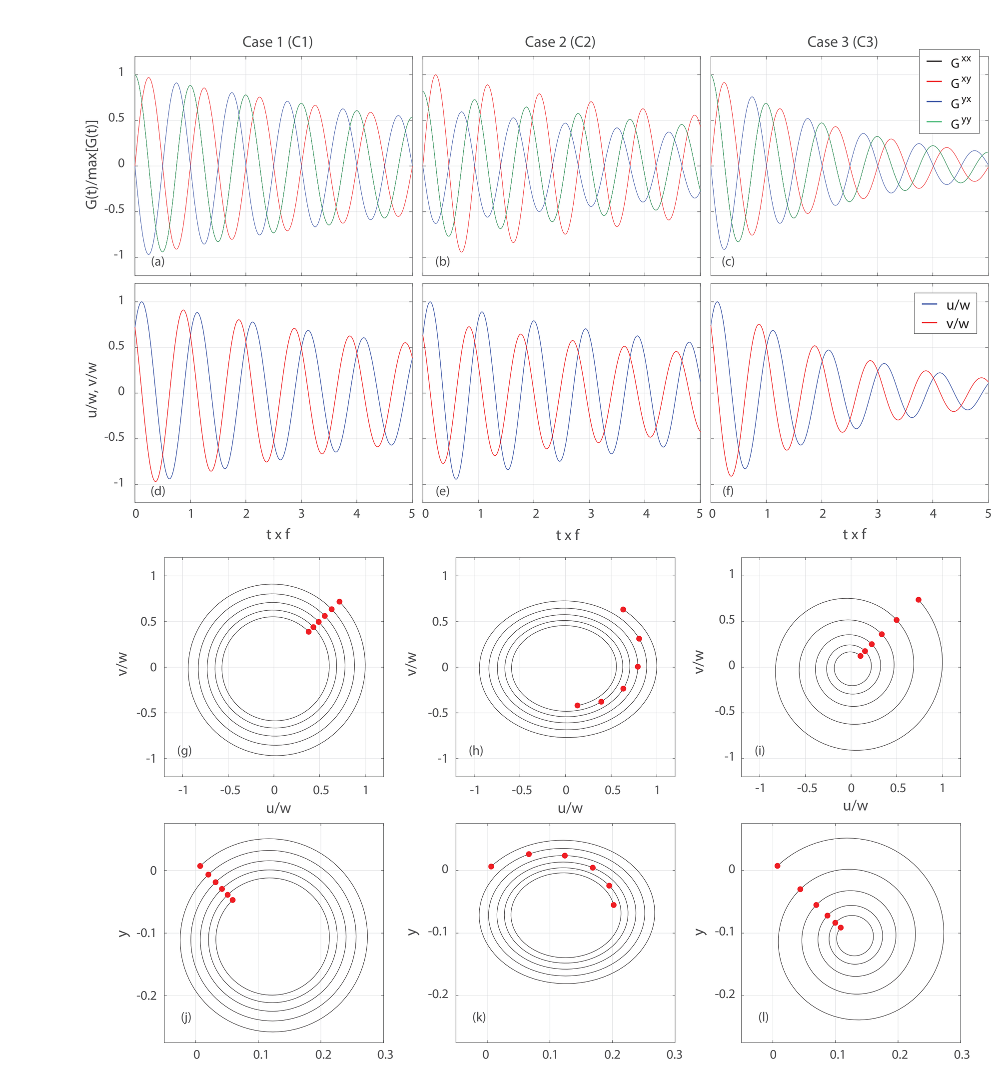

Figure 4: Response functions [$G(t)$; G^{xx}, G^{xy}, G^{yx}, and G^{yy}], and time series and hodographs of the current components (u/w and v/w) normalized by the maximum velocity [w; $w = \max\left(\sqrt{u(t)^2 + v(t)^2}\right)$], and the spatial trajectories (x and y) under horizontal strain components (u_x and v_y), horizontal shear components (v_x and u_y), and frictional coefficients (r^x and r^y). (a), (d), (g), and (j): $r^x = 0.1f$ and $r^y = 0.15f$. (b), (e), (h) and (k): $r^x = 0.1f$, $r^y = 0.15f$, $u_y = -0.35f$, and $v_x = -0.15f$. (c), (f), (i), and (l): $r^x = 0.1f$, $r^y = 0.15f$, $u_x = 0.35f$, and $v_y = 0.15f$. Note that G^{xx} and G^{yy} in (a) to (c) are overlapped.

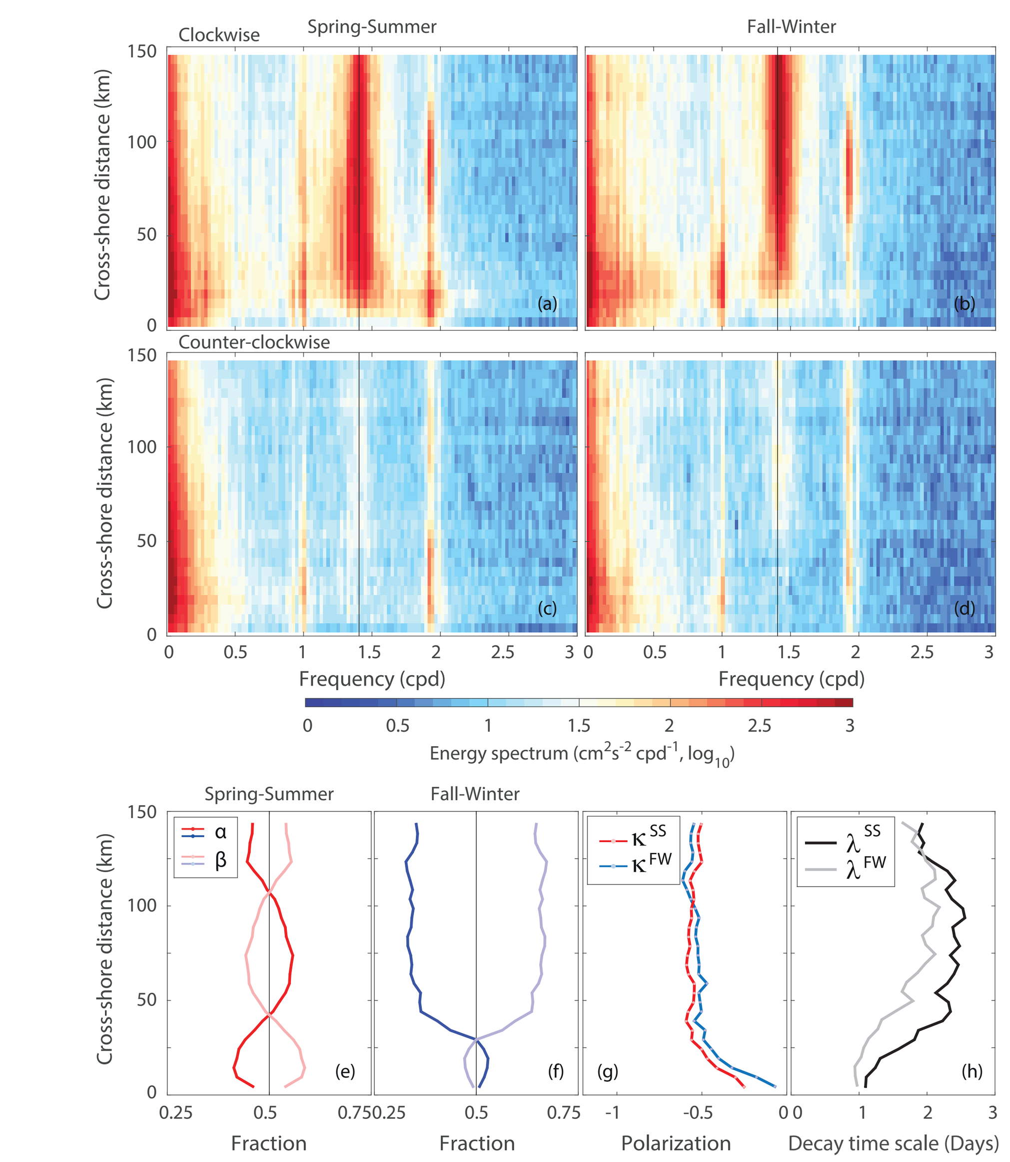

Figure 5: (a) to (d): Seasonal kinetic energy spectra of the HFR-derived surface currents sampled along the NH10 in [(a) and (c)] spring and summer (SS) and [(b) and (d)] fall and winter (FW) for a period of four years (2007 to 2010) in the [(a) and (b)] clockwise and [(c) and (d)] counter-clockwise frequency as a function of cross-shore distance. (e) and (f): Fractions of the variance in the sub-inertial (α; thicker) and super-inertial (β; paler) frequency bands normalized by total near-inertial variance in SS (red) and FW (blue). (g) Seasonal polarizations (κ^{SS} and κ^{FW}) of the near-inertial surface currents in the cross-shore direction. (h) Decay time scales (λ^{SS} and λ^{FW}, days) of the near-inertial surface currents in SS (black) and FW (gray). Note that the black vertical lines in Figs. 5a to 5d denote the local Coriolis frequency ($f = 1.405$ cpd).

The variance within the near-inertial frequency band is expected to be unequally distributed when it is centered in terms of the local Coriolis frequency as a result of the shear components including vorticity. Thus, the super-inertial variance becomes dominant ($\alpha < \beta$) with positive vorticity (counter-clockwise; $\zeta > 0$), and the subinertial variance becomes dominant ($\alpha > \beta$) with negative vorticity (clockwise; $\zeta < 0$). The variances of the HFR-derived surface currents in spring and summer (SS) in the super-inertial and subinertial frequency bands become significant at distances less than 40 km and greater than 110 km from the coast and between 40 km and 110 km from the coast, respectively (Figs. 5a and 5e), which implies that the positive vorticity ($l < 40$ km and $l \ge 110$ km) and negative vorticity (40 km $\le l <$ 110 km) are dominant. In contrast, the variance ratios of the super-inertial and subinertial frequency bands in fall and winter (FW) exhibit their dominance at distances less and greater than 25 km from the coast, respectively, which implies that the negative vorticity ($l < 25$ km) and positive vorticity ($l \ge 25$ km) are dominant (Figs. 5b and 5f). The reduced polarization of the near-inertial surface currents persistently appears near the coast in both seasons because of the enhanced fraction of the counter-clockwise variance with respect to the clockwise variance close to the coast (Figs. 5a to 5d and 5g).

Acknowledgement

Sung Yong Kim is supported by the Khalifa University of Science, Technology and Research (KUSTAR)–Korea Advanced Institute of Science and Technology (KAIST) Institute, KAIST (SMP-N11190100), Republic of Korea. The satellite-tracked surface drifters are provided by NOAA AOML Global Drifter Program. The coastal radar-derived surface current data and numerical model outputs are provided by P. Michael Kosro and Alexander Kurapov in Oregon State University.